ChemPubSoc Europe

DOI: 10.1002/chem.201605102

CHEMISTRY A European Journal Full Paper

Ab Initio Calculations |*Hot Paper*|

Ab Initio Crystal Field for Lanthanides

Liviu Ungur*[a, b] and Liviu F. Chibotaru*[a]

Abstract: An ab initio methodology for the first-principle derivation of crystal-field (CF) parameters for lanthanides is described. The methodology is applied to the analysis of CF parameters in $[Tb(Pc)_2]^-$(Pc = phthalocyanine) and Dy_4K_2 ($[Dy^4K^2O(OtBu)^{12}]$) complexes, and compared with often used approximate and model descriptions. It is found that the application of geometry symmetrization, and the use of electrostatic point-charge and phenomenological CF models, lead to unacceptably large deviations from predictions based on ab initio calculations for experimental geometry. It is shown how the predictions of standard CASSCF (Complete Active Space Self-Consistent Field) calculations (with 4*f* orbitals in the active space) can be systematically improved by including effects of dynamical electronic correlation (CASPT2 step) and by admixing electronic configurations of the 5*d* shell. This is exemplified for the well-studied Er-trensal complex (H_3trensal = 2,2′,2″-tris(salicylideneimido)trimethylamine). The electrostatic contributions to CF parameters in this complex, calculated with true charge distributions in the ligands, yield less than half of the total CF splitting, thus pointing to the dominant role of covalent effects. This analysis allows the conclusion that ab initio crystal field is an essential tool for the decent description of lanthanides.

Introduction

The crystal field (CF) of lanthanide ions in complexes or in crystals is the main characteristic defining the structure of luminescence bands and magnetic properties.[1–7] Several descriptions of this kind have been proposed, taking into account the electrostatic field splitting (Stark effect)[8–10], and the weak covalence splitting (angular overlap model)[11–13] of the 4f atomic levels. To incorporate both these effects, hybrid versions of crystal-field models have also been proposed. These include the superposition model,[14,15] the effective charge model,[16] the simple overlap model,[17] and the mixed covalo-electrostatic model.[18]

A rapidly increasing interest for new lanthanide complexes, observed in recent years,[19,20] prompted several research groups to put forward new computational tools for the investigation of crystal field in lanthanides, such as the recently developed SIMPRE[21] and PHI packages,[22] both based on electrostatic models. Phenomenological crystal-field models are also currently in use.[5,8] The bottleneck of all these approaches is the large number of independent parameters (27 in low-symmetric complexes) required for the description of the crystal field, which cannot all be extracted from experiment. In practice only four to five parameters, at most, can be extracted from the fitting of magnetic and spectroscopic experimental data.[23–29] Extraction of larger number of crystal-field parameters, in low symmetry complexes is problematic because of over-parameterization of the fitting procedure, when several different sets of fitted parameters become equally acceptable, thus invalidating the whole procedure of their derivation. Another problem encountered by "classical" crystal-field models is the poor transferability of crystal-field parameters corresponding to individual ligands. This drawback has its roots in the complex distance and angular dependences of these parameters, even for monoatomic ligands.[30] As a result, the crystal-field models employed to date were necessarily oversimplified, emphasizing the role of axial crystal-field parameters B_k^0 (see below) over other parameters, even in low-symmetric complexes. Such over-simplification leads to unrealistic wave functions of crystal-field multiplets, which precludes efficient crystal-field treatment of lanthanides. In particular, incorrect parameterizations from assumed symmetry, or naive point-charge models hold back the research area of molecular magnetism, spectroscopy, etc., by essentially providing misleading theoretical insight.

Recently, ab initio methods have proved to be a reliable tool for the description of low-lying multiplets of lanthanide complexes with experimental accuracy.[31,32] They allowed the de-

[a] *Dr. L. Ungur, Prof. Dr. L. F. Chibotaru*
Theory of Nanomaterials Group, Department of Chemistry, and Institute of Nanoscale Physics and Chemistry -INPAC
Katholieke Universiteit Leuven
Celestijnenlaan 200F
3001 Leuven (Belgium)
E-mail: Liviu.Ungur@chem.kuleuven.be
Liviu.Chibotaru@chem.kuleuven.be

[b] *Dr. L. Ungur*
Theoretical Chemistry Group
Department of Chemistry
Lund University
Getingevagen 60
22100, Lund (Sweden)
E-mail: Liviu.Ungur@chem.kuleuven.be

Supporting Information and the ORCID identification number(s) for the author(s) of this article can be found under http://dx.doi.org/10.1002/chem.201605102.

scription from first principles of the magnetism of transition metal and lanthanide complexes,[33–36] and to derive the zero-field splitting and Zeeman interactions in terms of pseudospin operators, corresponding to chosen multiplets.[31,32] This calculation methodology was implemented in the basic ab initio package MOLCAS[37–39a], and used for the rationalization of magnetic properties in many strongly anisotropic metal complexes. A natural extension of this methodology would be an ab initio derivation of the crystal field in complexes, first of all in lanthanides. A fully ab initio methodology of the derivation of crystal-field parameters is presented, describing the splitting of the ground atomic *J*-multiplet of Ln ions. The basic feature of the proposed approach is that all crystal-field parameters are derived in a unique way, that is, without use of any fitting procedure, contrary to their extraction from experiment. Therefore, applying this ab initio methodology, it can be ensured a priori that the "true" crystal field of the complex is derived[39b]. Of course, the obtained set of parameters is exact only if the low-lying ab initio spectrum is exact as well.

It should be mentioned here that several attempts of projection of ab initio results on simple ligand-field (crystal-field) theories have been made in the past. They employed density functional theory[40] and multireference methods.[41,42] The unifying line of these methods is that they attempt to parameterize the entire energy spectrum of the lanthanide from the performed calculations. The main point of the present approach is that it does not attempt to parameterize the entire energy spectrum of the lanthanides, but rather concentrate on accurate extraction of the crystal-field describing the splitting of their ground *J*-multiplet. The projection technique presented here takes into account the wavefunctions and energies of all crystal-field states (all calculated ab initio) to define the parameters of the crystal field of the ground *J*-multiplet.

Results and Discussion

Ab initio methodology for crystal field

The crystal field acting on an electronic shell, *nl*, of a lanthanide ion is given by Equation (1):[43]

$$\widehat{H}_{CF} = \sum_{i} \sum_{k,q} \boldsymbol{B}_k^q \boldsymbol{O}_k^q(\theta_i, \varphi_i) \tag{1}$$

where $O_k^q(\theta_i, \varphi_i)$ is the Stevens operator dependent on angular coordinates (θ_i, φ_i) defined in a given coordinate system, B_k^q is the crystal-field parameter of rank $k = 2, 4, 6$ for $nl = 4f$, q is the projection of the operator, and i numbers the electrons. Projected on the ground atomic multiplet $^{2S+1}L_J$ of the lanthanide ion, Equation (1) transforms into Equation (2):[43]

$$\widehat{H}_{CF} = \sum_{k,q} \alpha_n \boldsymbol{B}_k^q \boldsymbol{O}_k^q(\boldsymbol{J}) \tag{2}$$

where α_n is the Stevens projection coefficient, whereas $O_k^q(J)$ is the Stevens operator acting on the eigenfunctions of the total angular momentum of the ground state. Here, the operators O_k^q are the Hermitean combinations of spherical harmonics: $O_k^{q,c} = \frac{1}{2}(Y_k^{-q} + (-1)^q Y_k^q)$; $O_k^{q,s} = \frac{i}{2}(Y_k^{-q} - (-1)^q Y_k^q)$.[31]

The crystal-field Hamiltonian [Eq. (2)] describes the splitting of the ground atomic multiplet into $2J+1$ levels, which are pairwise degenerate for half-integer *J*, that is, for Kramers ions. This spectrum should be compared with the lowest $2J+1$ levels of the complex, obtained in ab initio calculations with spin-orbit coupling included, from which the parameters B_k^q can in principle be extracted. In practice it is not possible to remain confined to energy levels, since the number of their differences, even for the largest angular momentum $J = 8$, is by far smaller than 27, the number of independent crystal-field parameters in the case of low symmetry complexes (the most common situation in lanthanides). Therefore, for a rigorous derivation of crystal-field parameters ab initio and crystal-field wave functions should be compared as well. This can be easily done by comparing the ab initio and crystal-field energy matrices written in equivalent basis of multiplet wave functions. The latter means that ab initio wave functions are put in correspondence to crystal-field wave functions. Note that the wave functions in both basis sets are not required to be eigenfunctions of the problem, that is, the energy matrices are not necessarily diagonal. Finding such correspondence for arbitrary wave functions of low symmetry complex is a non-trivial problem, which is discussed in detail in Ref. [32], where a derivation of crystal field for lanthanides is also described. Here the problem is approached in a simple way by making use of very weak metal–ligand hybridization of 4*f* orbitals in lanthanide complexes.

It is well known that the atomic *J*-multiplet splits, in an applied homogeneous magnetic field, into $2J+1$ Zeeman levels, corresponding to definite projections, *M*, of the total angular momentum on the direction of the field. Hence, diagonalizing the Zeeman matrix of the complex, written in the basis of lowest $2J+1$ ab initio wave functions Ψ_n, we can put in correspondence the eigenfunctions of individual Zeeman levels, $\tilde{\Psi}_p = \sum_{n=1}^{2J+1} c_{p_n} \Psi_n$, to eigenfunctions $|JM\rangle$ corresponding to definite projections *M* of the total angular momentum on the direction of applied field. Moreover, given that the three *g* factors of the entire manifold of $2J+1$ states do not differ much from the Landé factor g_J of the corresponding ground-state atomic multiplet of the Ln ion,[43] all three *g* factors are ensured to be positive, a priori.[44] This means that the lowest Zeeman level always corresponds to $M = -J$, whereas the highest one corresponds to $M = J$. Next, the energy matrix corresponding to the lowest $2J+1$ ab initio eigenfunctions Ψ_n, containing only energies E_n on its diagonal, is rewritten into the basis of Zeeman eigenstates $\tilde{\Psi}_p$. Then, given the correspondence between $\tilde{\Psi}_p$ and $|JM\rangle$, each element of this energy matrix, $\langle \tilde{\Psi}_{p_1} | \widehat{H} | \tilde{\Psi}_{p_2} \rangle = \sum_{i=1}^{2J+1} c_{p_1 i}^* c_{p_2 i} E_i$, with the matrix element $\langle JM_1 | H_{CF} | JM_2 \rangle \equiv (H_{CF})_{M_1 M_2}$ of the crystal-field Hamiltonian in Equation (2), can be identified. Next, the crystal-field parameters B_k^q defining H_{CF} are obtained through the simulation of the obtained energy matrix. To this end the irreducible tensor operator (ITO) technique is employed, which projects the crystal-field energy matrix onto the matrices of Stevens operators $O_k^q(J)$, written in the basis of crystal-field states $|JM\rangle$. The coef-

ficients of this decomposition, when divided by the corresponding Stevens parameters α_n, are precisely the crystal-field parameters B_k^q. The described ITO procedure is equivalent to the one used for the ab initio derivation of parameters of zero-field splitting (ZFS) in magnetic molecules;[31,32] therefore, the same expressions were used for the coefficients of projection, Equations (32), (39), and (41) from Ref. [32], in which $(H_{ZFS})_{M_1M_2}$ should be replaced by $(H_{CF})_{M_1M_2}$.This methodology was already implemented in the SINGLE_ANISO module of the MOLCAS ab initio package.[38] The implementation provides crystal-field parameters for a desired coordinate frame (quantization axis). Parameters are reported for several forms of crystal-field Hamiltonian. The values of all 27 crystal-field parameters entering Equation (2) are given together with the crystal-field wave functions.

An evident advantage of the described procedure is that it provides a unique set of crystal-field parameters B_k^q. This is in sharp contrast to the fitting procedures, which give several sets of crystal-field parameters. Furthermore, there is freedom to define the parameters B_k^q with respect to arbitrary coordinate system, despite the fact that experimental structural data (the crystallographic information file, CIF) is used by default in the ab initio calculations. First, the atomic coordinates in the ab initio calculation may be chosen in any desired coordinate frame. Secondly, even when the ab initio calculation is done on the basis of the CIF, the passage to the desired coordinate system may be further carried out with the use of the corresponding rotation matrices in the SINGLE_ANISO program. The program's default coordinate frame is the main magnetic axes of the ground multiplet of the complex, in which the direction corresponding to g_Z is chosen as quantization axis. The term "unique", used above, means that one single set of B_k^q parameters, which fully reproduces the energy matrix of the ground *J*-multiplet, is derived for a given coordinate system. The set of parameters corresponding to another coordinate frame may be obtained by standard transformations of the initial set by employing the Wigner functions.[45]

A second important advantage of the developed ITO methodology is the possibility to evaluate also the contribution of higher rank operators $O_k^q(J)$, with $k = 8, 10, \leq 2J$, which go beyond the standard crystal-field theory. The values of the corresponding crystal-field parameters B_k^q for $k \geq 8$ allow the quantitative assessment of the applicability of the crystal-field approach to lanthanides, which can only be considered valid if all higher rank ($k \geq 8$) B_k^q are negligible. When this is not the case, it should be concluded that the covalent admixture of ligand orbitals to the 4*f* orbitals is not small.

The ab initio calculations of lanthanide complexes presented here have been carried out with the MOLCAS package. In the approach used, relativistic effects are taken into account in two steps, both based on the Douglas–Kroll Hamiltonian.[46–48] In the first step, scalar relativistic effects are already taken into account in the basis set generation.[49,50] Next, spin-free eigenstates are obtained in the Complete Active Space Self-Consistent Field (CASSCF) method,[51,52] as implemented in MOLCAS.[37,53] The active space of CASSCF included only electrons spanning seven 4*f* orbitals of the Ln^{3+} ion. In the second step, spin-orbit coupling is taken into account within the space of calculated spin-free eigenstates using the RASSI module.[54] In this approach, the spin-orbit coupling is described in the Atomic Mean Field approximation (AMFI).[55] The obtained spin-orbit multiplets, corresponding to exact electronic states of the complex, were used for the calculation of crystal-field parameters, within the methodology described above, using the module SINGLE_ANISO.[38]

Ab initio vs. phenomenological crystal-field models

First Ishikawa's double-decker terbium phthalocyanine complex $[Tb(Pc)_2]^-$ (Figure 1).[23,24] The structure of this complex

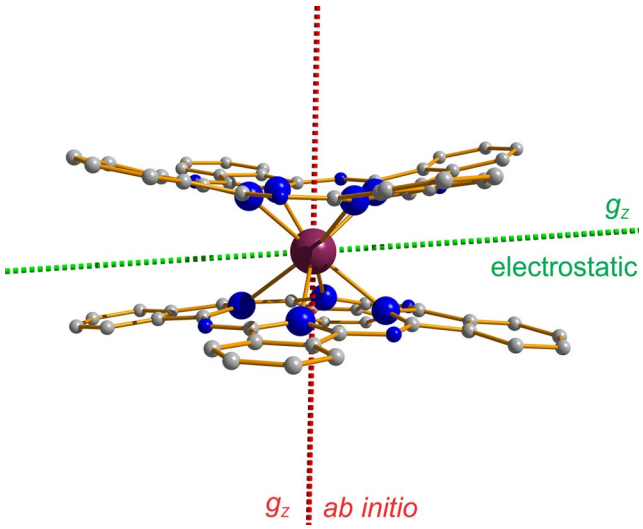

Figure 1. Main magnetic axis of the ground doublet of the $[Tb(Pc)_2]^-$ anion obtained from ab initio calculation (red dashed line). The green dashed line shows the main magnetic axis obtained within the electrostatic model employing Mulliken point charges.

does not possess strict symmetry, however it is close to the D_{4d} point group. In the latter case only three axial terms ($\sim B_k^0, k = 2, 4, 6$) are permitted by symmetry, facilitating the application of phenomenological crystal-field models. Figure 2 shows the result of ab initio calculations for experimental and symmetrized (D_{4d}) geometries, as well as the predictions of phenomenological crystal-field models by Ishikawa et al.[23,24], and Reu et al.[56] The main difference in the two phenomenological models lies in the chosen symmetry of the compound, which has a great influence on the allowed parameters in the crystal-field Hamiltonian employed. Ishikawa et al.[23,24] assumed that the $[Tb(Pc)_2]^-$ compound has a D_{4d} symmetry, whereas Reu et al.[56] considered a lower point group symmetry of the compound, namely C_4, with a more complex form of the employed crystal-field Hamiltonian, and more fitting parameters in the phenomenological approach.

The X-ray structure of the $[Tb(Pc)_2]^-$ anion employed in ab initio calculations was taken from a recent publication.[57] Contractions of the basis sets describing individual atoms in ab initio calculations are given in the Supporting Information. Ab

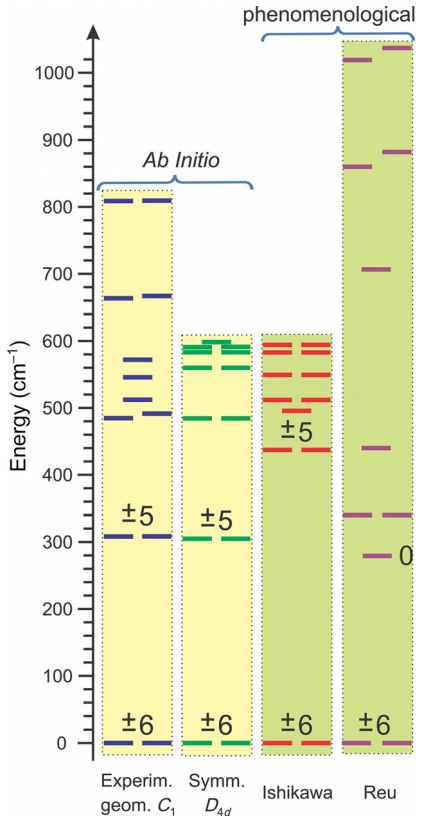

Figure 2. Comparison of the crystal-field spectrum, corresponding to the ground atomic multiplet of Tb^{3+} in the $[Tb(Pc)_2]^-$ anion, obtained ab initio for experimental and symmetrized-D_{4d} structures, with the spectra obtained in the phenomenological crystal-field models of Ishikawa et al.[23,24] (assuming the exact D_{4d} symmetry), and Reu et al.[56] (assuming C_4 symmetry). The numbers stand for the M_J projection of the total angular moment in the corresponding states of the main magnetic axis of the ground doublet (red dashed line in Figure 1).

initio calculations were of CASSCF/RASSI/SINGLE_ANISO kind using an active space of CAS(8 in 7) which included the $4f^8$ shell of the Tb^{3+} central ion. 7 spin septets, 106 spin quintets, 283 spin triplets and 121 spin singlets were mixed by spin-orbit coupling within RASSI, resulting in 1517 spin-orbit states. The ab initio obtained eigenstates corresponding to the ground multiplet $J=6$ of Tb^{3+}, were further employed in the procedure described above for the computation of crystal-field parameters. All spin-orbit states were employed for the computation of the ab initio calculated magnetic susceptibility χT. Table 1 lists the corresponding crystal-field parameters, while Figure 3 shows the comparison between ab initio calculated[38] and measured[23,24] magnetic susceptibility. Table S3 (in the Supporting Information) shows the weight of individual rank crystal-field parameters in the total crystal-field splitting for this compound.

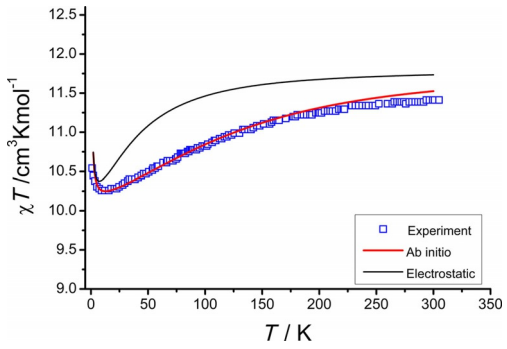

Figure 3. Comparison between calculated point-charge electrostatic model (black line), ab initio (red line), and measured magnetic susceptibility for the $[Tb(Pc)_2]^-$ anion. A mean-field intermolecular interaction parameter, $zJ=0.01$ cm^{-1}, was introduced to account for the weak ferromagnetic coupling between $[Tb(Pc)_2]^-$ anions in the crystal; it is mainly responsible for the upturn of the calculated χT curve in the low-temperature region (2–9 K).

Table 1. Ab initio and phenomenological crystal-field parameters B_k^q (in cm^{-1}) for the $[Tb(Pc)_2]^-$ anion.[a]

k	q	Ab initio, experimental geometry		Ab initio, *D4d*-symmetrized geometry		Fitting by Ishikawa et al., ref. [23,24]		Fitting by Reu et al., ref. [56]	
		Re	Im	Re	Im	Re	Im	Re	Im
	0	608.8	–	530.4	–	414.0	–	173.0	–
2	1	−19.1	4.6	0.0	0.0	x	x	x	x
	2	19.2	317.9	0.0	0.0	x	x	x	x
	0	−98.5	–	−112.0	–	−228.0	–	−631.4	–
	1	−11.0	0.5	0.0	0.0	x	x	x	x
4	2	3.5	59.8	0.0	0.0	x	x	x	x
	3	0.6	−2.2	0.0	0.0	x	x	x	x
	4	−15.0	5.0	0.0	0.0	x	x	397.4	953.0
	0	−13.9	–	−7.5	–	33.0	–	79.7	–
	1	−0.2	−0.9	0.0	0.0	x	x	x	x
	2	−0.7	24.1	0.0	0.0	x	x	x	x
6	3	1.3	−1.2	0.0	0.0	x	x	x	x
	4	−5.3	3.0	0.0	0.0	x	x	256.4	667.0
	5	3.4	−4.1	0.0	0.0	x	x	x	x
	6	12.1	17.9	0.0	0.0	x	x	x	x

[a] $Re = \frac{1}{2}(B_k^{-q} + (-1)^q B_k^{+q})$, $Im = \frac{i}{2}(B_k^{-q} - (-1)^q B_k^{+q})$—real and imaginary part, respectively, of the crystal-field parameters; x = parameters neglected in the phenomenological models.[23,24,56]

As can be seen from Table 1, the ab initio crystal-field parameters corresponding to the experimental and symmetrized-D_{4d} geometries differ drastically; notably by the presence of large imaginary components in the former case. The obtained large differences in the two sets of crystal-field parameters seem surprising, given the relatively small variations of the real geometry from the symmetrized one. This shows that the symmetrization of geometry should be avoided for a realistic description of lanthanide complexes. Figure 2 shows large deviations of the spectra given by phenomenological crystal-field models (except for the nature of the ground doublet) from ab initio predictions for experimental geometry. The model by Ishikawa et al.[23,24] correctly predicts the $mJ = \pm 5$ nature of the first excited doublet, which places it at a significantly higher energy than the ab initio one (430 vs. 308 cm^{-1}); the latter value being much closer to the experimentally extracted magnetization blocking barrier (260 cm^{-1}).[23,24] Another observation is the strong mixing of the $|J,M\rangle$ states, corresponding to different M, in the multiplets lying above the second doublet in the spectrum, corresponding to the real geometry, which is inferred from the analysis of the corresponding crystal-field wave functions, carried out with the SINGLE_ANISO module (Table S2). Such a mixing is not expected for a D_{4d} crystal-field and serves as additional evidence for the very high sensitivity of spin-orbit multiplets of lanthanide complexes to small changes in their geometry.

Ab initio crystal-field vs. point-charge electrostatic models

Another important issue, which can be clarified by the present ab initio approach, is the relative strength of electrostatic contributions to the crystal field in lanthanide complexes. Here, the effect of atomic point charges extracted from quantum chemistry calculations is considered; the full treatment of electrostatic contribution to the crystal field, based on true distribution of the electronic charge in the ligands, will be discussed in a subsequent section. First, the effect of atomic point charges on the ground crystal-field multiplet are analyzed, for which the $[Tb(Pc)_2]^-$ anion is again considered (Figure 1).

Due to the sandwich structure of the complex, the crystal field contains axial and equatorial components of comparable strength. The ab initio calculation (first column in Figure 2) gives the direction of the main magnetic axis of the ground doublet perpendicular to the plane of two phtalocyanines, which points to a dominant role of the axial component of crystal field. The electrostatic-field calculation using the Mulliken atomic charges of all atoms surrounding Tb^{3+} in the $[Tb(Pc)_2]^-$ complex (see Supporting Information for details) gives the main magnetic axis for the ground doublet deviating by 86° from the ab initio result (Figure 1). This testifies to the modified relative strengths of axial and equatorial components to the crystal field in the electrostatic calculations, which turned out to be sufficient to dramatically change the properties of the ground crystal-field doublet of the complex. In the lack of clearly determined direction of the axial crystal field, either as a symmetry axis or a strongly coupled atom from the ligand environment, the direction of the main magnetic axis predicted by the electrostatic model can deviate significantly from its actual direction. This conclusion is valid not only for the case of point charges but refers to electrostatic models in general. Moreover, the computed magnetic susceptibility for the Tb^{3+} ion in the field of atomic point charges deviates clearly from both the experimental and ab initio calculated curves (Figure 3).

To assess the effect of point-charge electrostatic interaction on the spectrum of crystal-field multiplets, an opposite case of a complex with a pronounced axial crystal field, arising from a strong interaction of Ln^{3+} ions with one of the ligand atoms, was considered. Figure 4 shows ab initio and electrostatic crystal-field splitting for low-symmetry Dy^{III} sites in a Dy_4K_2 complex ($[Dy_4K_2O(OtBu)_{12}]$).[58] In this investigation, the ligand atoms in the four fragments, Dy1–Dy4, were simulated by their calculated Mulliken charges, obtained in previous ab initio calculations.[58] Structures of the computed fragments and the computed values of the atomic charges are given in the Supporting Information (Tables S7–S10). Table S4 gives the ab initio and electrostatic calculated energy spectra of the ground $J = 15/2$ multiplet of the Dy fragments. Table S14 shows the ab initio derived crystal-field parameters for both cases, ab initio and electrostatic, in the same coordinate frame. The crystal-field splitting of the ground $J = 15/2$ of the Dy^{3+} site is reduced by almost three times in the case when atoms are simulated by physically meaningful point charges. Given that the ab initio calculations have been carried out on the CASSCF level, that is, no dynamical correlation was included, the obtained atomic Mulliken charges are expected to be slightly ex-

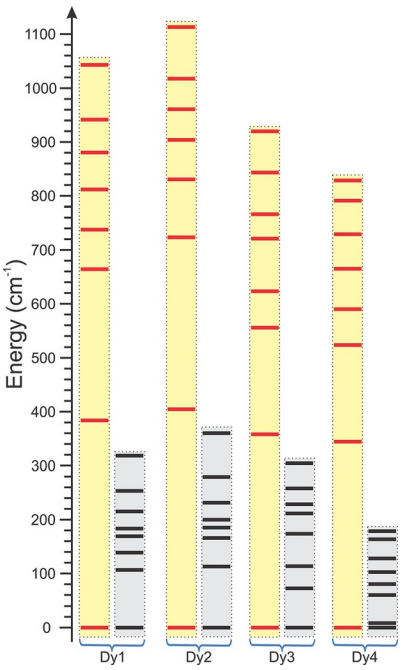

Figure 4. Ab initio (red lines) and point-charge electrostatic (black lines) crystal field splitting on Dy sites in the Dy_4K_2 complex.[58] Numerical values of ab initio and electrostatic energies shown here are provided in Table S4.

aggerated, whereas the covalence of Ln-ligand bonds are slightly underestimated. The same is expected for the covalent and electrostatic contribution to the crystal field, respectively, although their sum gives a crystal field that usually describes the experiment satisfactorily, especially for the low-lying crystal-field multiplets.[35,36] Given this observation, the electrostatic contribution to the crystal field may be even smaller than that calculated above, that is, not dominant, at least for the archetypal Ln-complexes considered. It is clear from Figure 4 that, to approach the spread of ab initio crystal-field levels, the charges of surrounding atoms (or of the closest ones to the Ln ion) should be significantly increased over their physical values, that is, they should be considered a priori as fictitious ones. Of course, no knowledge of the values of these charges exists in advance, nor their variations among non-equivalent ligand atoms. This makes the corresponding electrostatic crystal-field models intrinsically phenomenological,[8–10,14–16,18] lacking, in particular, predictive power as for other phenomenological models.[59]

High-accuracy ab initio calculation of the crystal field

The accuracy of the predicted crystal field is crucially dependent on the quality of ab initio calculations. In this respect the ab initio methods have a clear advantage over phenomenological models and semi-empirical quantum chemistry approaches (including DFT), as their results can be systematically improved on a rigorous basis by increasing the level of computation. Thus, the standard state-average CASSCF/SO-RASSI approach used in the previous sections, which proved to be a reasonably accurate tool for the description of the magnetism in the majority of lanthanide complexes,[60] can be further improved by enlarging the active space and by including the dynamical electronic correlation (the CASPT2 step). Such increase of computational level is especially important for accurate evaluation of the whole crystal-field spectrum. Indeed, the CASSCF level, usually sufficient for a decent description of the ground and low-lying crystal-field states (mostly responsible for the magnetism of the complexes), often underestimates the energies of the excited crystal-field states.

The factors which can be varied within the CASSCF/CASPT2/RASSI calculations are as follows:

1) Basis sets describing the individual atoms. Larger basis sets have more variational degrees of freedom, thus providing more accurate results.
2) The size of the active space of the CASSCF/RASSCF method. Larger active spaces usually improve the results, but care has to be taken on the selection of orbitals included in the active space.
3) Dynamical electron correlation, namely, the effect of singly and doubly excited configurations not included in CASSCF are accounted for perturbatively by the CASPT2 method.[61,62]
4) Number of spin states included in the spin-orbit interaction within RASSI.
5) Account of the interaction effects of the neighboring molecules, and Madelung electrostatic potential from the whole crystal.

A comprehensive benchmark study of all these factors is out of the scope of the present manuscript. However, the yet unexplored effect of the dynamical correlation on the crystal-field splitting of the ground *J*-multiplet for lanthanide complexes is presented here for the first time. For this benchmark study the well-known Er-trensal complex (H_3trensal = 2,2′,2″-tris(salicylideneimido)trimethylamine) was chosen (Figure S2 in Supporting Information and Figure 8 below).[35,63,64]. For this compound, the description of magnetic properties, and of the crystal-field spectrum, proved to be insufficiently accurate at the CASSCF level. This compound has been well investigated by experimental means. Thus the low-lying energy spectrum was experimentally extracted from luminescence measurements.[63,64] In addition, a few low-lying transitions were confirmed by inelastic neutron scattering (INS).[35] Magnetic properties of this compound were probed by electron paramagnetic resonance (EPR) and also by single-crystal magnetic measurements.[35]

All calculations were based on the experimental structure of the Er-trensal complex,[35] determined at 293 K. Atomic coordinates of the Er-trensal compound employed for this study are given in Table S11 (Supporting Information). Er, O, N, and C atoms close to Er were described by ANO-RCC-VDZP basis sets. More distant C and H atoms were described by the same basis without polarization. A total of 35 spin quartet states were optimized within a state-average CASSCF calculation, and mixed by the spin-orbit coupling within RASSI. The CASPT2 calculations, based on the corresponding CASSCF states, made use of the recently implemented XMS feature.[65,66] It should be noted that the conventional CASPT2 method is not able to preserve exact degeneracies. For lanthanide free ions, the spurious splitting of exactly degenerate states of the atomic *J*-multiplet is of the same order of magnitude as the crystal-field splitting arising due to ligands' environment. This makes the conventional CASPT2 approach rather inapplicable for the calculation of the low-lying part of the crystal-field splitting in lanthanides. In contrast, the XMS-CASPT2 version[65,66] (recently implemented in the MOLCAS/CASPT2 program) does not suffer from this problem. In the CASPT2 calculations, the IPEA shift[67] was set to 0.0 Ha (in place of the default 0.25 Ha) and the imaginary shift was set to 0.1 Ha to avoid intruder state problems; the multistate coupling procedure (computation of the off-diagonal matrix elements between first-order corrected CASPT2 states) was skipped, as it is not yet parallelized and therefore cannot be performed routinely for large multi-root calculations (keyword NOMULT was employed for this purpose). The CASPT2 default for the number of frozen orbitals was kept unaltered.

Table 2 shows the results of the ab initio calculations with varying levels of accuracy in comparison with the spectrum of crystal-field multiplets extracted from luminescence measurements. Figure 5 shows selected calculated spectra plotted alongside the experimentally derived data. Table S13 shows the crystal-field parameters describing the splitting of the

Table 2. Low-lying energy spectrum (in cm^{-1}) and g factors of the ground Kramers doublet of Er-trensal obtained by CASSCF/CASPT2/RASSI computation.

CASPT2	−	+	−	+	
Effect from neighbour molecules[a]	−	−	+	+	
	CASSCF active space: CAS(11 in 7), ($4f^{11}$ shell).				
Model	A1	A2	A3	A4	Exp.[35,63,64],[a]
1	0.0	0.0	0.0	0.0	0
2	61.4	83.4	53.4	75.7	54
3	100.9	140.3	92.2	129.4	102
4	101.3	149.1	97.0	145.0	110
5	211.2	359.4	213.3	362.7	299
6	413.1	607.1	404.6	597.8	568
7	454.8	677.0	447.1	668.8	610
8	482.9	724.1	473.9	713.2	642
g_X	2.33	3.13	2.80	3.82	3.36
g_Y	2.33	3.17	2.80	3.87	3.36
g_Z	13.69	12.60	13.05	11.58	11.90
	CASSCF active space: CAS(11 in 14), ($4f^{11}+5f^0$ shell).				
Model	B1	B2	B3	B4	Exp.[35,63,64],[a]
1	0.0	0.0	0.0	0.0	0
2	69.7	80.5	60.5	71.7	54
3	109.4	130.0	99.6	119.4	102
4	110.1	132.2	104.1	127.6	110
5	239.4	304.4	239.8	308.6	299
6	441.5	547.8	431.4	538.7	568
7	486.2	599.2	476.9	591.4	610
8	517.9	635.4	506.7	625.6	642
g_X	2.47	2.74	3.00	3.33	3.36
g_Y	2.47	2.75	3.00	3.35	3.36
g_Z	13.55	13.16	12.82	12.32	11.90
	RASSCF active space: CAS(17 in 25) (Ras1−$5p^6$, Ras2−$4f^{11}$, Ras3−$5f^0$, $5d^0$, and $6p^0$).[b]				
Model	C1	C2	C3	C4	Exp.[35,63,64],[a]
1	0.0	0.0	0.0	0.0	0
2	61.9	71.6	52.7	63.3	54
3	105.2	121.1	94.8	110.9	102
4	107.4	125.4	102.2	121.0	110
5	233.4	293.2	234.4	297.6	299
6	453.7	534.2	443.9	525.2	568
7	499.1	582.4	490.1	574.6	610
8	528.8	613.3	518.0	603.9	642
g_X	2.50	2.77	3.08	3.42	3.36
g_Y	2.50	2.78	3.09	3.45	3.36
g_Z	13.49	13.08	12.68	12.14	11.90

[a] Electrostatic effect of the crystal (Madelung potential) was modeled by Mulliken atomic charges of five layers of surrounding unit cells of molecules. [b] Configurations with maximum two holes in Ras1 and maximum two electrons in Ras3 were allowed.

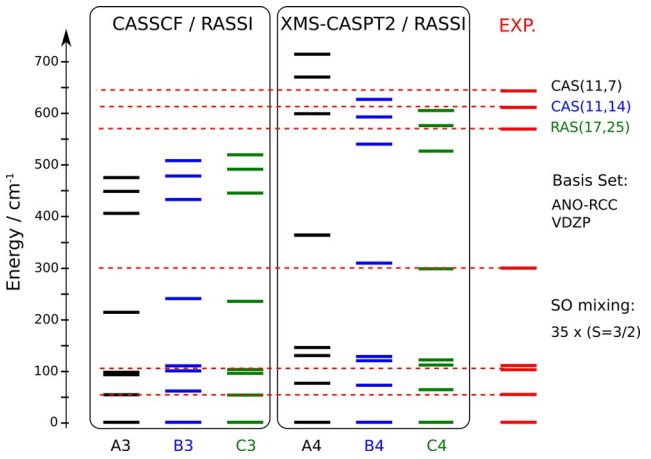

Figure 5. A comparison between various ab initio approaches to the calculation of the crystal field spectrum of Er-trensal, with data extracted from luminescence.[63] All ab initio calculations included the Madelung potential. Labels stand for specific computational models listed in Table 2.

ground $J=15/2$ for Er-trensal in the initial coordinate system for all computational models presented here. The models A1 and A3 in Table 2 show close agreement with previously reported ab initio results on this compound,[35] albeit employing a larger basis set. The Madelung electrostatic field of the crystal has a similar effect in all computational models; it reduces the energies of Kramers doublets 2, 3, 4, 6, 7, and 8 by ca. 5–10 cm^{-1}, and increases the energy of Kramers doublet 5 by ca. 2–5 cm^{-1}. A more noticeable effect of the Madelung potential is seen on the g tensor of the ground Kramers doublet: g_X and g_Y values increase significantly, whereas g_Z is strongly decreasing.

Despite relative good agreement for the lowest three excitation energies of the A3 model, the total splitting (473 cm^{-1}) is clearly underestimated compared to the measured one (642 cm^{-1}). In all cases (models 2 and 4, all active spaces), the effect of dynamical correlation leads to an increase of the total splitting of the ground atomic $J=15/2$ of Er^{3+} compared to the corresponding CASSCF/RASSI results. In the case of minimal active space (models A2, A4), the increase of the crystal field splitting is larger than the measured one; an effect attenuated by larger active spaces. The increase of the total splitting has as the drawback of a poorer description of the low-lying excited states. A similar trend is noticed for the transversal g factors of the ground Kramers doublet, $g_{X,Y}$, which become larger than their uncorrelated equivalents, whereas the effect of the Madelung potential makes the $g_{X,Y}$ even larger than the experimental ones.

The increase of the active space by the addition of the double shell—another set of seven metal-based f orbitals—leads to a noticeable improvement of the results (models B2 and B4). In these cases, the total splitting of the ground $J=15/2$ multiplet is in almost perfect agreement with the total splitting obtained experimentally. Even more, a correct trend for the excitation energies of all Kramers doublets is noticed. The calculated g tensor of the ground Kramers doublets is also in an almost ideal agreement with experimental data. By increasing the active space, some of the dynamical correlation at the CASSCF level is actually included, and so the "overshooting" effect of the CASPT2 is not seen anymore, which is a nice point of this approach. The same is true for the ground state g tensor.

Finally, the active space was further increased by including $5p^6$, $5d^0$, $6p^0$, and $5f^0$ orbital configurations in addition to the minimal active space. Because the number of CI configurations becomes very large for such an extended active space, we em-

ployed the RAS restrictions (see Table 2). RASPT2 calculations[61,62] were performed on top of the optimized RASSCF wave functions. Since more of the dynamical correlation is accounted for at the RASSCF level, an increase of the total splitting for models C1 and C3 (uncorrelated) is noticeable compared to smaller active spaces A1, A3, B1, and B3, respectively, corroborated by an increase of the $g_{X,Y}$ values for the ground Kramers doublet. This is clearly an effect of additional dynamical correlation included at the RASSCF level. As a result, there is less correlation to be included at the RASPT2 level of theory and consequently, smaller differences between the C models, and B and A models, respectively.

Figure 6 shows a comparison between measured single-crystal and powder temperature dependence of the magnetic susceptibility and calculated one in various computational models discussed here. Please note the improved agreement for the models B4 and C4 (employing CASPT2 and Madelung potential) with experimental data.

It can be concluded that the dynamical correlation effects for lanthanide compounds is a necessary ingredient for accurate estimation of the crystal-field spectrum, and magnetic/electronic properties of individual crystal-field doublets of lanthanide complexes, provided that the active space of the CASSCF method is chosen large enough (like in models B or C) to counteract the overshooting effect of the second-order perturbation theory seen for the minimal active spaces. Given the small energy differences in the crystal-field levels of lanthanides, the electrostatic weak effect of the crystal (the Madelung potential) also plays an important role for improving the overall accuracy.

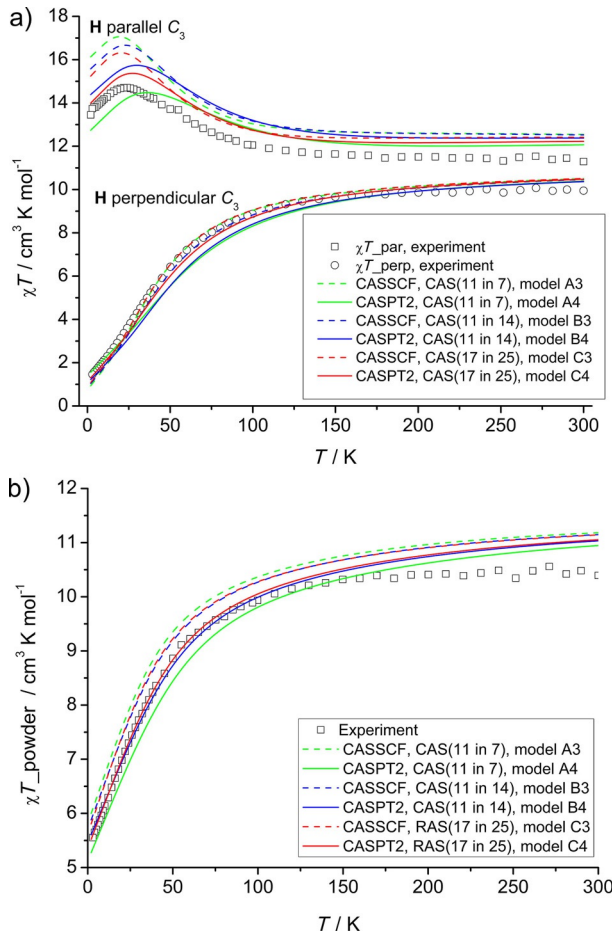

Figure 6. a) Comparison between measured and calculated magnetic susceptibility for Er-trensal for cases when magnetic field is aligned parallel and perpendicular to the C_3 symmetry axis. b) Comparison between measured and calculated powder magnetic susceptibility for Er-trensal. The discrepancy between theoretically predicted magnetic susceptibility and measured one in the temperature domain 200–300 K is attributed to the fact that in all calculations reported here the spin doublet states were not included. The relative larger discrepancy for χT at perpendicular orientations of the applied field is proportional to the larger deviations of g_X and g_Y from experiment. Misalignment of the single-crystal magnetic measurements could also be a reason for the noticed deviations.

Ab initio crystal-field vs. electrostatic models based on true charge distribution

Several recent studies promoted the idea that the crystal field of the lanthanides is dominated by the electrostatic contribution,[68–71] or claim that the ground state is dominantly influenced by electrostatic effects of the ligands.[72] Although the effect of the electrostatic field from physical (Mulliken) point charges has been analyzed in a previous section, this assumption was further verified using a precise description of the electrostatic potential from the ligands. The Er-trensal compound was again used for this purpose. In the first approach, each atom of the ligand was simulated again by a point charge (Mulliken and LoProp[73] charges) obtained in a previous DFT or SCF/MP2 calculation of the ligand taken alone (with the charge −3). In the second approach, the true space distribution of the electronic density in the ligand was considered explicitly in the calculation of the electrostatic potential. This distribution was simulated by a large collection of point charges (ca. 2.9×10^6 point charges). In this approach, an iterative procedure was applied where the electronic densities of the ligand and of the lanthanide ion (also represented as a collection of a large number of point charges) were optimized self-consistently. The electronic density of the ligand was found by a Hartree–Fock calculation on the ligand $(trensal)^{3-}$, whereas the electronic density of the Er^{3+} was obtained within a CASSCF calculation. The electronic density of the $(trensal)^{3-}$ ligand was included in the calculation of the metal and vice-versa iteratively until self-consistency between the two potentials was achieved. CASSCF/RASSI energies of the lanthanide ion, in the field of the optimal converged potential of the ligand, are reported below (Table 3). Finally, the last non-covalent approach employed the previously developed Fragment Ab Initio Model Potential method (FAIEMP) implemented in MOLCAS program package.[74] In this approach two fragments were considered: the metal and the ligand. Ab initio calculations on individual fragments were performed until the two electronic densities (represented by the molecular orbitals in their own basis set expansion, occupation numbers, and orbital energies) were adjusted to each other through a self-consistent procedure. The difference of this approach from the second one is that it includes two other non-covalent interactions besides the electro-

Table 3. Crystal field spectrum and *g* factors of the ground Kramers doublet of Er-trensal obtained with electrostatic models and the minimal CASSCF/RASSI calculation.

	(*trensal*)$^{3-}$ ligand represented by:			
Ab initio[a]	DFT (B3LYP) Mulliken atomic charges	SCF/MP2 Mulliken atomic charges	Electrostatic potential of true charge distribution (2.9×10^6 point charges)	Fragment AIMP
Crystal field levels of atomic $J=15/2$ multiplet [cm^{-1}]				
0.0	0.0	0.0	0.0	0.0
61.4	9.0	4.5	19.8	6.3
100.9	23.2	19.0	47.9	43.8
101.3	33.2	30.1	91.0	90.1
211.2	37.0	34.0	123.9	160.6
413.1	64.0	74.8	151.4	188.9
454.8	65.5	76.9	214.8	201.1
482.9	66.8	78.2	241.3	243.3
g factors				
2.33	0.001	0.005	9.900	7.712
2.33	0.001	0.007	7.368	7.348
13.69	17.417	17.164	2.528	4.035

[a] A1 model in Table 2.

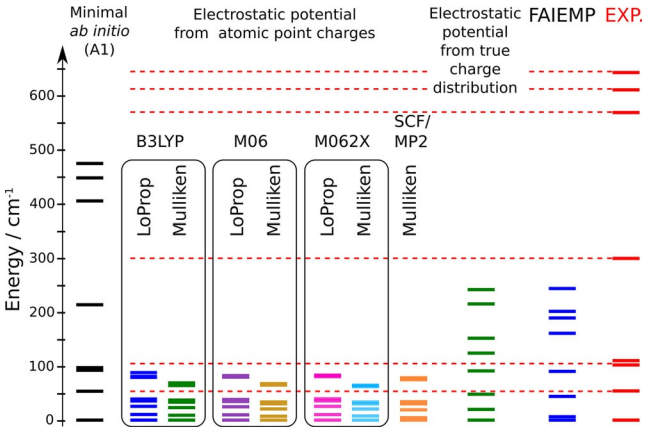

Figure 7. Comparison of predictions of various electrostatic models and the minimal CASSCF calculation (A1 in Table 2) of the crystal field spectrum of Er-trensal.

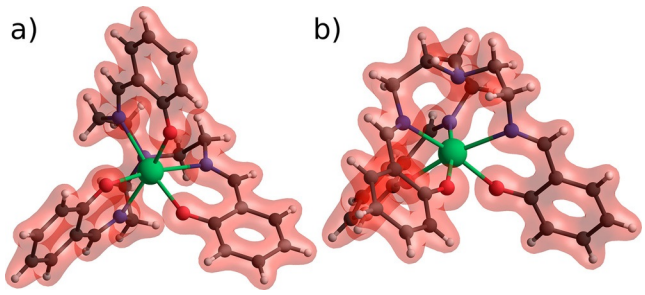

Figure 8. Two views (a,b) of the distribution of electronic density of the (trensal)$^{3-}$ ligand surrounding Er^{3+} in the Er-trensal.

static one; the exchange interaction between the ligand and the metal electrons, and the Pauli's repulsion contribution originating from the requirement of orthogonality between metal and ligand molecular orbitals bearing electrons of the same projection of spin. The latter interaction prevents, in particular, over-delocalization of metallic electrons in the core regions of ligand atoms. For this reason the FAIEMP approach represents the most rigorous non-covalent embedding of a metal ion in the potential created by the ligand. Table 3 shows the results of CASSCF/RASSI calculations of crystal-field splitting of $J=15/2$ on Er^{3+} in various electrostatic and non-covalent potentials of the (trensal)$^{3-}$ ligand. The active space of the CASSCF method included only the $4f^{11}$ shell of the Er^{3+}. For consistency, the basis sets and all other computational details were kept similar to the A1 model in the previous section.

Figure 7 shows that the crystal-field splitting of the 4*f* shell of the Er^{3+} ion, in the electrostatic field generated by physical point charges of 62 ligands' atoms, is more than six times smaller than the experimental crystal-field splitting. The values of the calculated atomic LoProp and Mulliken charges are given in the Supporting Information (Tables S11 and S12). The space distribution of the electronic charge of the (trensal)$^{3-}$ ligand is shown in Figure 8 and the corresponding crystal-field splitting of the ground atomic multiplet $J=15/2$ of the Er^{3+} ion is given in Figure 7. It amounts to approximately 40% of the experimental crystal-field splitting extracted from the luminescence data. The same is true for the electronic density embedding within the FAIEMP method[74] (Figure 7), which points to a dominant role of the electrostatic field among the non-covalent contributions to the crystal-field splitting.

As can be inferred from Figure 7, all non-covalent approaches to the crystal-field of the Er^{3+} ion coordinated by three (trensal)$^{3-}$ ligands fail dramatically. To achieve a realistic crystal-field splitting within "electrostatic" models, artificial modifications of true (physical) electrostatic potential are required, by either increasing the point charges on nearest-neighbor ligand atoms, or by lowering the metal–ligand distance, or even by displacing the point charges arbitrarily from the metal–ligand axis.[71] These modifications make the models phenomenological, since they do not try to simulate the effect of a true electrostatic potential arising from ligands, but merely represent a version of parameterization of the crystal-field parameters B_k^q. At variance to them, the ab initio calculations, even in their simplest (standard) CASSCF/RASSI version with a minimal active space, without taking into account the effects of Madelung potential, and dynamical electron correlation, already provide a splitting of the ground $J=15/2$ of Er^{3+} amounting to 75% of the experimental value. As Table 2 and Figure 5 show, the missing 25% of the crystal-field splitting is recovered by the lacking effects of dynamical electronic correlation and Madelung potential. The reason for significantly larger crystal-field splitting in the CASSCF/RASSI calculations compared to various true electrostatic models, is that the ab initio methods allow for the mixing between metal and the ligand orbitals, giving rise to covalent contributions to the crystal field. It is a well-known fact of post Hartree–Fock methods, that the metal–ligand covalence is underestimated at the

CASSCF level, requiring a larger active space (RASSCF), and inclusion of dynamical electron correlation (CASPT2 step) for a decent description. This tendency is clearly observed also in the calculated crystal-field splitting (Figure 7).

It is instructive to reveal the effect of true electrostatic potential on the *g* tensor of the ground crystal-field multiplet. A particular interest for such inquiry is sparked by the often used argument that matching orientations of main magnetic axes (corresponding to the largest *g*-factor, g_Z) obtained by ab initio calculations and electrostatic models, is a proof of dominant electrostatic contribution to the crystal field in lanthanides.[57] To this end, the *g* factors of Er-trensal were calculated with various approaches. Given a very close geometry of Er-trensal to the C_3 point group, the orientation of the main magnetic axis obtained ab initio, and by any electrostatic models, always match each other, because the latter should be aligned to the C_3 rotational axis for ideal trigonal geometry. Despite the good matching of the orientations of the calculated main magnetic axes, Table 3 shows that the electrostatic point-charge models are giving a very axial *g* tensor for the ground doublet, in complete disagreement with experiment. In contrast, the electrostatic models based on true space distribution of the electronic charge in the ligands, including FAIEMP, predict easy-plane type magnetic anisotropy of the ground-state *g* tensor in a major disaccord with experiment (Table 2). Notably, neither of the electrostatic approaches are able to correctly describe the magnetic behavior of this compound, $\chi(T)*T$ and $M(T,H)$. At the same time, the minimal ab initio CASSCF/RASSI calculation (model A1 in Table 2) gives the ground-state *g* tensor much closer to the experimental values. As inferred from Table 2, the addition of dynamical electron correlation and Madelung potential leads to solutions that are very close to experiment.

Conclusions

The ab initio methodology for the investigation of the crystal field in lanthanide complexes presented here offers two major advantages over other approaches employed so far. First, it allows derivation of all 27 crystal-field parameters in a unique way. Second, it takes into account all contributions to the crystal field, and allows the analysis of their relative strengths. These advances permit the application of crystal-field analysis in a more insightful way than earlier phenomenological approaches.

The role of the electrostatic contribution to the crystal field in lanthanides were analyzed in detail, using (i) atomic point charges (Mulliken, LoProp) derived from quantum chemistry calculations, and (ii) true space distribution of the electronic charge in the ligands. The thoroughly investigated example of the Er-trensal complex shows that the electrostatic potential yields less than half of the strength of the crystal field; the main contribution being provided by covalency effects. Also, the magnetism of this complex and, especially, the anisotropic properties of the ground Kramers doublet, cannot be correctly reproduced by electrostatic models.

The possibility of enhancing the accuracy of the calculated crystal-field multiplets was also investigated. It was shown that inclusion of the effects of dynamical electron correlation (lacking in the conventional CASSCF approach), together with the electrostatic Madelung potential of the crystal, lead to a much closer agreement between measured and calculated energies, and the anisotropic magnetic properties of individual crystal-field multiplets (Table 2 and Figure 5). This suggests that ab initio crystal field calculations are likely to become an essential tool for accurate description of optical and magnetic properties of lanthanide complexes.

The developed method to extract crystal-field information from rigorous ab initio calculations can be, in principle, directly applied for the investigation of the crystal field in actinides, provided the ab initio calculations for them is done at the proper level. In this respect, accurate benchmarking of the ab initio computational strategy for crystal fields in actinide compounds is required.

Finally, it should be emphasized that the ab initio based methods are advancing fast, with significant improvements in recent years in terms of accuracy and speed. When combined with the fast advancement of the processing power, and development of novel computer architectures, these methods gradually become more and more important for chemical research, by providing predictive insight into various studies.

Acknowledgements

L.U. is a postdoc supported by the FWO (Fonds Wetenschappelijk Onderzoek—Vlaanderen). The support of the Concerted Research Action (GOA) of KU Leuven is gratefully acknowledged. Prof. P.-Å. Malmqvist is gratefully acknowledged for useful discussions.

Keywords: ab initio calculations · covalent interactions · electrostatic models · lanthanides · single-molecule magnets

[1] S. V. Eliseeva, J.-C. G. Buenzli, *Chem. Soc. Rev.* **2010**, *39*, 189 – 227.
[2] K. Binnemans, *Chem. Rev.* **2009**, *109*, 4283 – 4374.
[3] Y. J. Cui, Y. F. Yue, G. D. Qian, B. L. Chen, *Chem. Rev.* **2012**, *112*, 1126 – 1162.
[4] R. Sessoli, A. K. Powell, *Coord. Chem. Rev.* **2009**, *253*, 2328 – 2341.
[5] B. G. Wybourne, L. Smentek, *Optical Spectroscopy of Lanthanides: Magnetic and Hyperfine Interactions*, CRC, Boca Raton, **2007**.
[6] V. K. Pecharsky, K. A. Gschneidner, Jr., *J. Magn. Magn. Mater.* **1999**, *200*, 44 – 56.
[7] a) Please note, in the case of lanthanides, the term "crystal field" is widely used instead of the more chemical "ligand field. b) S. T. Liddle, J. van Slageren, *Chem. Soc. Rev.* **2015**, *44*, 6655 – 6669.
[8] J. Mulak, Z. Gajek, *The effective crystal field potential*, Elsevier, Amsterdam, **2000**.
[9] H. Bethe, *Ann. Phys.* **1929**, *395*, 133 – 206.
[10] C. Rudowicz, S. K. Misra, *Appl. Spectrosc. Rev.* **2001**, *36*, 11 – 63.
[11] C. E. Schäffer, C. K. Jørgensen, *Mol. Phys.* **1965**, *9*, 401 – 412.
[12] B. N. Figgis, M. A. Hitchman, *Ligand field theory and its applications*, Wiley-VCH, Weinheim, **2000**.
[13] W. Urland, *Chem. Phys.* **1976**, *14*, 393 – 401.
[14] M. I. Bradbury, D. J. Newman, *Chem. Phys. Lett.* **1967**, *1*, 44 – 45.
[15] D. J. Newman, *Adv. Phys.* **1971**, *20*, 197 – 256.
[16] C. A. Morrison, R. P. Leavitt in *Handbook on the Physics and Chemistry of Rare Earths, Vol. 5* (Eds.: K. A. Gschneidner, Jr., L. Eyring), North-Holland Publishing Company, Amsterdam, **1982**, pp. 461.

[17] O. L. Malta, S. J. L. Ribeiro, M. Faucher, P. Porcher, *J. Phys. Chem. Solids* **1991**, *52*, 587 – 593.
[18] D. Garcia, M. Faucher, *J. Chem. Phys.* **1985**, *82*, 5554 – 5564.
[19] D. N. Woodruff, R. E. P. Winpenny, R. A. Layfield, *Chem. Rev.* **2013**, *113*, 5110 – 5148.
[20] J. Rocha, L. D. Carlos, F. A. A. Paz, D. Ananias, *Chem. Soc. Rev.* **2011**, *40*, 926 – 940.
[21] J. J. Baldoví, S. Cardona-Serra, J. M. Clemente-Juan, E. Coronado, A. Gaita-Ariño, A. Palii, *J. Comput. Chem.* **2013**, *34*, 1961 – 1967.
[22] N. F. Chilton, R. P. Anderson, L. D. Turner, A. Soncini, K. S. Murray, *J. Comput. Chem.* **2013**, *34*, 1164 – 1175.
[23] N. Ishikawa, M. Sugita, T. Ishikawa, S. Koshihara, Y. Kaizu, *J. Am. Chem. Soc.* **2003**, *125*, 8694 – 8695.
[24] N. Ishikawa, M. Sugita, T. Ishikawa, S. Koshihara, Y. Kaizu, *J. Phys. Chem. B* **2004**, *108*, 11265 – 11271.
[25] M. A. AlDamen, J. M. Clemente-Juan, E. Coronado, C. Marti-Gastaldo, A. Gaita-Ariño, *J. Am. Chem. Soc.* **2008**, *130*, 8874 – 8875.
[26] M. A. AlDamen, S. Cardona-Serra, J. M. Clemente-Juan, E. Coronado, A. Gaita-Ariño, C. Marti-Gastaldo, F. Luis, O. Montero, *Inorg. Chem.* **2009**, *48*, 3467 – 3479.
[27] F. Luis, M. J. Martínez-Pérez, O. Montero, E. Coronado, S. Cardona-Serra, C. Martí-Gastaldo, J. M. Clemente-Juan, J. Sesé, D. Drung, T. Schurig, *Phys. Rev. B* **2010**, *82*, 060403.
[28] K. Katoh, T. Kajiwara, M. Nakano, Y. Nakazawa, W. Wernsdorfer, N. Ishikawa, B. K. Breedlove, M. Yamashita, *Chem. Eur. J.* **2011**, *17*, 117 – 122.
[29] L. Sorace, C. Benelli, D. Gatteschi, *Chem. Soc. Rev.* **2011**, *40*, 3092 – 3104.
[30] V. Nekvasil, *Czech. J. Phys.* **1979**, *29*, 785 – 796.
[31] L. F. Chibotaru, L. Ungur, *J. Chem. Phys.* **2012**, *137*, 064112.
[32] L. F. Chibotaru, in *Advances in Chemical Physics, Vol. 153* (Eds. S. A. Rice, A. R. Dinner), Wiley, Hoboken, **2013**, pp. 397 – 519.
[33] L. F. Chibotaru, L. Ungur, C. Aronica, H. Elmoll, G. Pilet, D. Luneau, *J. Am. Chem. Soc.* **2008**, *130*, 12445 – 12455.
[34] L. F. Chibotaru, L. Ungur, A. Soncini, *Angew. Chem. Int. Ed.* **2008**, *47*, 4126 – 4129; *Angew. Chem.* **2008**, *120*, 4194 – 4197.
[35] K. S. Pedersen, L. Ungur, M. Sigrist, A. Sundt, M. Schau-Magnussen, V. Vieru, H. Mutka, S. Rols, H. Weihe, O. Waldmann, L. F. Chibotaru, J. Bendix, J. Dreiser, *Chem. Sci.* **2014**, *5*, 1650 – 1660.
[36] R. Marx, F. Moro, M. Dörfel, L. Ungur, M. Waters, S. D. Jiang, M. Orlita, J. Taylor, W. Frey, L. F. Chibotaru, J. van Slageren, *Chem. Sci.* **2014**, *5*, 3287 – 3293.
[37] F. Aquilante, L. De Vico, N. Ferre, G. Ghigo, P. A. Malmqvist, P. Neograd, T. B. Pedersen, M. Pitonak, M. Reiher, B. O. Roos, L. Serrano-Andrés, M. Urban, V. Veryazov, R. Lindh, *J. Comput. Chem.* **2010**, *31*, 224 – 247.
[38] F. Aquilante, J. Autschbach, R. K. Carlson, L. F. Chibotaru, M. G. Delcey, L. De Vico, I. F. Galván, N. Ferre, L. M. Frutos, L. Gagliardi, M. Garavelli, A. Giussani, C. E. Hoyer, G. Li Manni, H. Lischka, D. Ma, P. A. Malmqvist, T. Müller, A. Nenov, M. Olivucci, T. B. Pedersen, D. Peng, F. Plasser, B. Pritchard, M. Reiher, I. Rivalta, I. Schapiro, J. Segarra-Marti, M. Stenrup, D. G. Truhlar, L. Ungur, A. Valentini, S. Vancoillie, V. Veryazov, V. P. Vysotskiy, O. Weingart, F. Zapata, R. Lindh, *J. Comput. Chem.* **2016**, *37*, 506 – 541.
[39] a) L. Ungur, L. F. Chibotaru, SINGLE_ANISO module, see: http://www.molcas.org/documentation/manual. b) The term "true" is used in the sense of "unique" for the particular ab initio calculation performed. This means that, contrary to the traditional extraction of CF parameters from experiment, a methodology is proposed to find them in a unique way.
[40] M. Atanasov, P. Comba, C. A. Daul, *Inorg. Chem.* **2008**, *47*, 2449 – 2463.
[41] L. F. Chibotaru, M. F. A. Hendrickx, S. Clima, J. Larionova, A. Ceulemans, *J. Phys. Chem. A* **2005**, *109*, 7251 – 7257.
[42] M. Atanasov, D. Ganyushin, K. Sivalingam, F. Neese, in *Structure and Bonding, Vol. 143* (Eds.: D. M. P. Mingos, P. Day, J. P. Dahl), Springer, Berlin, **2012**, pp. 149 – 220.
[43] A. Abragam, B. Bleaney, *Electron Paramagnetic Resonance of Transition Ions*, Clarendon, Oxford, **1970**.
[44] L. F. Chibotaru, L. Ungur, *Phys. Rev. Lett.* **2012**, *109*, 246403.
[45] D. A. Varshalovich, A. N. Moskalev, V. K. Khersonskii, *Quantum Theory of Angular Momentum*, World Scientific, Singapore, **1988**.
[46] M. Douglas, N. M. Kroll, *Ann. Phys.* **1974**, *82*, 89 – 155.
[47] B. A. Hess, *Phys. Rev. A* **1986**, *33*, 3742 – 3748.
[48] M. Reiher, *Wiley Interdiscip. Rev.: Comput. Mol. Sci.* **2012**, *2*, 139 – 149.
[49] B. O. Roos, R. Lindh, P. Å. Malmqvist, V. Veryazov, P. O. Widmark, *J. Phys. Chem. A* **2005**, *109*, 6575 – 6579.
[50] T. Tsuchiya, M. Abe, T. Nakajima, K. Hirao, *J. Chem. Phys.* **2001**, *115*, 4463 – 4472.
[51] P. E. M. Siegbahn, J. Almlöf, A. Heiberg, B. O. Roos, *J. Chem. Phys.* **1981**, *74*, 2384 – 2396.
[52] J. Olsen, B. O. Roos, P. Jørgensen, H. J. A. Jensen, *J. Chem. Phys.* **1988**, *89*, 2185 – 2192.
[53] P.-Å. Malmqvist, A. Rendell, B. O. Roos, *J. Phys. Chem.* **1990**, *94*, 5477 – 5482.
[54] P.-Å. Malmqvist, B. O. Roos, B. Schimmelpfennig, *Chem. Phys. Lett.* **2002**, *357*, 230 – 240.
[55] B. A. Hess, C. M. Marian, U. Wahlgren, O. Gropen, *Chem. Phys. Lett.* **1996**, *251*, 365.
[56] O. S. Reu, A. V. Palii, S. M. Ostrovsky, P. L. W. Tregenna-Piggott, S. I. Klokishner, *Inorg. Chem.* **2012**, *51*, 10955 – 10965.
[57] F. Branzoli, P. Carretta, M. Filibian, G. Zoppellaro, M. J. Graf, J. R. Galan-Mascaros, O. Fuhr, S. Brink, M. Ruben, *J. Am. Chem. Soc.* **2009**, *131*, 4387 – 4396.
[58] R. J. Blagg, L. Ungur, F. Tuna, J. Speak, P. Comar, D. Collison, W. Wernsdorfer, E. J. L. McInnes, L. F. Chibotaru, R. E. P. Winpenny, *Nat. Chem.* **2013**, *5*, 673 – 678.
[59] J. van Leusen, M. Speldrich, H. Schilder, P. Kögerler, *Coord. Chem. Rev.* **2015**, *289*, 137 – 148.
[60] "Computational modelling of magnetic properties of lanthanide compounds": L. Ungur, L. F. Chibotaru in *Lanthanides and Actinides in Molecular Magnetism, Vol. 6* (Eds.: R. A. Layfield, M. Murugesu), Willey-VCH, Weinheim, **2015**, pp. 153 – 184.
[61] P.-Å. Malmqvist, K. Pierloot, A. R. M. Shahi, C. J. Cramer, L. Gagliardi, *J. Chem. Phys.* **2008**, *128*, 204109.
[62] S. Vancoillie, M. G. Delcey, R. Lindh, V. Vysotskiy, P.-Å. Malmqvist, V. Veryazov, *J. Comput. Chem.* **2013**, *34*, 1937 – 1948.
[63] B. M. Flanagan, P. V. Bernhardt, E. R. Krausz, S. R. Lüthi, M. J. Riley, *Inorg. Chem.* **2001**, *40*, 5401 – 5407.
[64] B. M. Flanagan, P. V. Bernhardt, E. R. Krausz, S. R. Lüthi, M. J. Riley, *Inorg. Chem.* **2002**, *41*, 5024 – 5033.
[65] A. A. Granovsky, *J. Chem. Phys.* **2011**, *134*, 214113.
[66] T. Shiozaki, W. Gyorffy, P. Celani, H.-J. Werner, *J. Chem. Phys.* **2011**, *135*, 081106.
[67] G. Ghigo, B. O. Roos, P. Å. Malmqvist, *Chem. Phys. Lett.* **2004**, *396*, 142 – 149.
[68] J. J. Baldoví, J. M. Clemente-Juan, E. Coronado, A. Gaita-Ariño, *Inorg. Chem.* **2014**, *53*, 11323 – 11327.
[69] D. Aravena, E. Ruiz, *Inorg. Chem.* **2013**, *52*, 13770 – 13778.
[70] I. Oyarzabal, J. Ruiz, J. M. Seco, M. Evangelisti, A. Camon, E. Ruiz, D. Aravena, E. Colacio, *Chem. Eur. J.* **2014**, *20*, 14262 – 14269.
[71] J. J. Baldoví, J. J. Borras-Almenar, J. M. Clemente-Juan, E. Coronado, A. Gaita-Ariño, *Dalton Trans.* **2012**, *41*, 13705 – 13710.
[72] N. F. Chilton, D. Collison, E. J. L. McInnes, R. E. P. Winpenny, A. Soncini, *Nat. Commun.* **2013**, *4*, 2551.
[73] L. Gagliardi, R. Lindh, G. Karlstrom, *J. Chem. Phys.* **2004**, *121*, 4494 – 4500.
[74] B. Swerts, L. F. Chibotaru, R. Lindh, L. Seijo, Z. Barandiaran, S. Clima, K. Pierloot, M. F. A. Hendrickx, *J. Chem. Theory Comput.* **2008**, *4*, 586 – 594.

Manuscript received: November 1, 2016
Accepted Article published: December 16, 2016
Final Article published: February 20, 2017